Published in final edited form as:
Neuron. 2013 December 18; 80(6): 1421–1437. doi:10.1016/j.neuron.2013.10.050.

Kinesin-1 Regulates Synaptic Strength by Mediating the Delivery, Removal and Redistribution of AMPA Receptors

Frédéric J. Hoerndli[*], **Dane A. Maxfield**[*], **Penelope J. Brockie**, **Jerry E. Mellem**, **Erica Jensen**, **Rui Wang**, **David M. Madsen**, and **Andres V. Maricq**[†]
Department of Biology, Center for Cell and Genome Science, University of Utah, Salt Lake City, UT 84112-0840

Summary

A primary determinant of the strength of neurotransmission is the number of AMPA-type glutamate receptors (AMPARs) at synapses. However, we still lack a mechanistic understanding of how the number of synaptic AMPARs is regulated. Here, we show that UNC-116, the *C. elegans* homolog of vertebrate kinesin-1 heavy chain (KIF5), modifies synaptic strength by mediating the rapid delivery, removal and redistribution of synaptic AMPARs. Furthermore, by studying the real-time transport of *C. elegans* AMPAR subunits *in vivo*, we demonstrate that although homomeric GLR-1 AMPARs can diffuse to and accumulate at synapses in *unc-116* mutants, glutamate-gated currents are diminished because heteromeric GLR-1/GLR-2 receptors do not reach synapses in the absence of UNC-116/KIF5-mediated transport. Our data support a model where ongoing motor-driven delivery and removal of AMPARs controls not only the number, but also the composition of synaptic AMPARs and thus the strength of synaptic transmission.

Introduction

The number of functional postsynaptic glutamate receptors is a major determinant of the strength of synaptic signaling. Thus, experience-dependent changes in the number of receptors contribute to fundamental network properties such as learning and memory (Jackson and Nicoll, 2011; Kerchner and Nicoll, 2008; Malinow and Malenka, 2002). Because most neurons have long processes, synapses are often far removed from the cell body, imparting a major challenge for the modulation and maintenance of synaptic machinery. While we have considerable insight into the local mechanisms that contribute to synaptic strength by regulating the recycling of AMPARs between the postsynaptic membrane and endosomal compartments (Henley et al., 2011; Kennedy and Ehlers, 2011; Kessels and Malinow, 2009; Petrini et al., 2009; Rusakov et al., 2011; Shepherd and Huganir, 2007; Yudowski et al., 2006), we have far fewer mechanistic insights into the long-range transport of AMPARs and how transport impacts synaptic strength and plasticity. These questions are particularly timely, considering the strong association of transport defects with synaptopathies and neurodegenerative disorders such as Alzheimer's disease (Stokin and Goldstein, 2006).

[†]Corresponding author (maricq@biology.utah.edu).
[*]These authors contributed equally to this work

At least three different mechanisms have been proposed for the long range delivery of AMPARs to synapses, including local synthesis (Ho et al., 2011; Ju et al., 2004), lateral diffusion (Adesnik et al., 2005) and motor dependent transport (Greger and Esteban, 2007; Kim and Lisman, 2001; Setou et al., 2002). However, it has been difficult to establish the relative contributions of these various processes to synaptic function. These competing models derive almost exclusively from *in vitro* studies in cultured neuronal preparations, and thus might not accurately reflect the effects of the local cellular environment, signaling molecules and the extracellular matrix, all of which can influence neuronal development and synaptic function. Therefore, we developed techniques that allowed us to directly observe the *in vivo* delivery of AMPARs to synapses in a specific neuron in *C. elegans*.

Studying AMPAR delivery in *C. elegans* allows us to integrate *in vivo* cell biological and electrophysiological studies of synaptic function. *C. elegans* are transparent and have only 302 neurons, a subset of which communicate by the synaptic release of glutamate to mediate specific behaviors (de Bono and Maricq, 2005). Glutamate gates a variety of receptors, including the GLR-1 AMPAR signaling complex, which is expressed in interneurons that contribute to worm locomotion (de Bono and Maricq, 2005). Previous studies have identified the molecular components of the GLR-1 signaling complex (Brockie et al., 2001; Mellem et al., 2002; Walker et al., 2006; Wang et al., 2012; Wang et al., 2008; Zheng et al., 2006; Zheng et al., 2004) and the mechanisms that regulate the localization and stability of synaptic GLR-1 (Burbea et al., 2002; Glodowski et al., 2007; Juo et al., 2007; Rongo and Kaplan, 1999; Rongo et al., 1998; Zhang et al., 2012).

We now demonstrate that the microtubule dependent motor, UNC-116/KIF5, and the associated kinesin light chain, KLC-2, mediate the transport of GLR-1 to synapses. In a series of *in vivo* studies, we evaluated the relative contributions of motor transport, receptor diffusion and local synthesis to the delivery of GLR-1 to synapses. We found that motor-mediated transport is the predominant mechanism for delivery, removal and redistribution of GLR-1. In *unc-116* mutants, GLR-1 diffused out of the cell body to proximal synapses, where it reached higher than normal levels secondary to the loss of motor-driven removal of synaptic receptors. Despite the synaptic accumulation of GLR-1 in *unc-116* mutants, glutamate-gated currents were severely diminished because the AMPAR signaling complex lacked GLR-1/GLR-2 heteromeric receptors. Defective AMPAR signaling in *unc-116* mutants was rescued by transient expression of UNC-116 in the adult nervous system, demonstrating that ongoing motor-dependent transport is required for the regulation of synaptic strength.

Results

In vivo measurement of GLR-1 transport

In *C. elegans*, the two AVA interneurons are part of a well-defined circuit that regulates worm reversal behavior. These neurons express the GLR-1 AMPAR subunit and each neuron extends a single process into the ventral cord that runs the length of the worm. We were able to specifically visualize these processes by using promoter sequences (*Prig-3* and *Pflp-18*) that limited transgene expression in the ventral cord to AVA (Figure S1A) (Feinberg et al., 2008; Wang et al., 2012). In transgenic worms that expressed a functional GFP-tagged variant of GLR-1 (GLR-1: :GFP) in AVA, we observed discrete GFP puncta, which mark postsynaptic sites along the processes (Figure S1B) (Rongo et al., 1998). To address how GLR-1 receptors are delivered to these synapses, we used real-time streaming confocal microscopy to image receptor movement. Unless otherwise indicated, we imaged a region of the proximal AVA process of young adult worms (Figure S1A, boxed region). To better image receptor transport, we first reduced background fluorescence by photobleaching a region of interest that was approximately 45 μm in length (Figure 1A). Transport events

were more apparent after photobleaching and we noted no adverse effects of photobleaching on transport (Figure S1C and S1D). We then captured a series of confocal images that revealed numerous small, fluorescent GLR-1: :GFP puncta that moved either anterogradely or retrogradely along the AVA processes. We refer to these as vesicles given that their movement was consistent with the known vesicular transport of transmembrane proteins (Figure 1B). The bidirectional vesicle transport, interrupted by occasional pauses or stops, is most apparent in kymographs generated from the full series of images (Figure 1C). The mobile vesicles were considerably smaller and dimmer than the large, immobile puncta (Figure 1D), which we refer to as synaptic puncta. Vesicles moved at approximately 1.6 μm/s in both anterograde and retrograde directions with an average run length of approximately 6 μm (Figure 1E).

Transport vesicles are directed to synapses

Most of the transport vesicles had brief pauses in their movement that were of variable duration (Figure 2A). A more detailed analysis of the kymographs revealed that stop events (defined as pauses in movement lasting at least 1.2 seconds) were clustered near existing GLR-1 synaptic puncta (Figures 2B and 2C). We also observed vesicles that stopped moving for extended periods, at times lasting many minutes. In one kymograph, we observed a vesicle moving anterogradely (Figure 2A, blue arrow) and another vesicle moving retrogradely (Figure 2A, red arrow), and observed both vesicles stop at the same synapse (Figure 2A, green box). Twenty minutes later, a kymograph of the same region revealed sustained recovery of GLR-1: :GFP fluorescence at the synapse where the two vesicles stopped (Figure 2A, lower panel, filled arrowhead), suggesting that these stops might have been permanent delivery events. We also detected long-lived increases in fluorescence at additional synapses (Figure 2A, lower panel, open arrowheads), which we assume reflect stoppage events that occurred in the twenty-minute interval between kymographs.

We next asked whether vesicles were delivered directly to the surface membrane, or first to a subsynaptic compartment. To simultaneously measure GLR-1 transport and surface delivery, we generated a transgenic strain that expressed a functional GLR-1 protein fused to both superecliptic pHluorin (SEP) and mCherry at the extracellular N-terminal domain (SEP: :mCherry: :GLR-1) (Kennedy and Ehlers, 2011) (Figure 2D). The SEP variant of GFP is pH sensitive and not appreciably fluorescent when localized to the relatively acidic environment of subcellular organelles in *C. elegans* (Dittman and Kaplan, 2006; Miesenbock et al., 1998; Wang et al., 2012). Thus, we rarely detect intracellular transport in the green channel (Figure 2E). Furthermore, photobleaching eliminates SEP fluorescence of surface GLR-1, but does not affect the SEP fluorophore on internalized receptors. Following photobleaching of both fluorophores, we acquired two-color streaming confocal movies to simultaneously monitor vesicle movement in the red channel and surface delivery of receptors that we detected by the appearance of a fluorescent signal in the green channel. Although we observed long-lived stops in vesicle movement, these were not immediately associated with GLR-1 surface delivery. However, we did observe insertion events occurring at variable intervals following vesicle stops (Figure 2E). This suggests that receptors were first delivered to a subsynaptic compartment rather than directly to the surface of the synapse, and that stoppage and insertion are separable processes. Insertion events were invariably at the same location as the synaptic puncta (Figure 2F and Figure S2A).

These data indicate that delivery of GLR-1 to synapses occurs in at least two steps. First, transport vesicles stop and deliver GLR-1 to a subsynaptic compartment in the region of a synapse. Second, after some delay, receptors are inserted into the synaptic membrane.

Interestingly, the insertion rate (Figure 2E) is a fraction of the stoppage rate (Figure 2C), even though the synaptic delivery (Figure S2B) and transport parameters (data not shown) were unaltered by the location of the fluorophore tag. This result suggests that not all longer duration stops (> 1.2 s) are destined for eventual insertion at a particular synapse.

GLR-1 receptors are redistributed between synapses

To determine the fate of GLR-1 receptors at synapses, we fused a photoactivatable florophore (PAGFP) to GLR-1 and expressed the functional protein in the AVA neurons. Following photoactivation of GLR-1: :PAGFP puncta, we occasionally observed vesicles leaving synaptic puncta and travelling in either an anterograde (Figure 3A) or retrograde (Figure 3A, insert) direction. These observations raised the question of whether GLR-1 receptors could be utilized at multiple synapses. We therefore evaluated the source of synaptic receptors using a photoconversion strategy to follow the fate of receptors from the cell body, and from proximal and distal synapses. We tagged GLR-1 with Dendra2, a photoconvertible fluorophore that can be switched from green to red fluorescence using UV illumination (Gurskaya et al., 2006) and expressed the functional fusion protein in the AVA neurons. Four hours after photoconversion of GLR-1: :Dendra2 in the AVA cell bodies, we found that approximately 25% of the fluorescent signal at distal synapses was red (Figure 3B). In contrast, we did not observe an appreciable red signal in the distal processes of sham-converted worms (Figure S3A).

Next, we photoconverted both synaptic puncta and interpunctal GLR-1: :Dendra2 fluorescence in the proximal region of the AVA processes. Fours hours after photoconversion, we monitored the appearance of red fluorescence at distal synapses and found that red signal originating in the proximal processes had been redistributed to distal puncta (Figure 3C). In separate experiments, we photoconverted only the synaptic puncta in the proximal processes, leaving the inter-puncta regions unconverted, and again observed red signal at distal synapses four hours after photoconversion (Figure 3D), but no red signal in sham-converted worms (Figure S3B). These data indicate that the red fluorescence, which appeared at distal synapses, was derived from receptors at proximal synapses rather than receptors that were photoconverted while in transit.

To further evaluate the redistribution of receptors, we photoactivated GLR-1: :PAGFP in the distal half of the AVA processes. Fours hours after photoactivation, we observed GLR-1: :PAGFP fluorescence at puncta in the proximal process (Figure 3E), but no signal in sham photoactivated controls (Figure S3C). Together, these data indicate that most synaptic GLR-1 receptors are delivered from the cell body to synapses, but receptors at a given synapse can be redistributed to other synapses.

UNC-116/KIF5 mediates GLR-1 transport

The speed and processivity of vesicle transport strongly suggested an energy-dependent, motor-driven process. In support of this hypothesis, we did not observe vesicle movement following treatment with Na-azide, a potent inhibitor of mitochondrial respiration and ATP production (Bowler et al., 2006), or nocodazole, an inhibitor of microtubule polymerization (Figure S3D), suggesting that microtubule-dependent motors drive the movement of GLR-1 vesicles. There are 21 known kinesin-like motors encoded by the *C. elegans* genome (Siddiqui, 2002), but only a few have been studied in detail, including OSM-3, UNC-104/KIF1, KLP-4 and UNC-116/KIF5. Of these, only UNC-104/KIF1 (kinesin-3), KLP-4 (a protein related to UNC-104) and UNC-116/KIF5 are known to be expressed in the AVA interneurons (Wormbase.org) (Siddiqui, 2002).

To determine the identity of the molecular motor(s) that transport GLR-1 receptors, we measured the *in vivo* transport of GLR-1: :GFP vesicles in candidate motor protein mutants and found that both anterograde and retrograde GLR-1 transport were dramatically disrupted in *unc-116* loss-of-function mutants (Figure 4A–4D). In contrast, we observed normal velocity and run length in *klp-4(ok3537)* null mutants and only mild disruption of transport in *unc-104(e1265)* null mutants (Figure S4A and S4B).

Interestingly, we observed an *unc-116* allelic series with respect to GLR-1: :GFP transport. Thus, the severity of the defects in GLR-1 transport speed, run length and the number of transport events progressively increased from *unc-116(e2310)* to *unc-116(rh24)* (Figure 4A–4D, Table S1). The defective GLR-1 transport observed in these *unc-116* partial loss-of-function mutants suggested that transport might be eliminated by a complete loss of UNC-116/KIF5 function. Unfortunately, we were unable to measure GLR-1 transport in null mutants because the *unc-116* null allele is lethal (Byrd et al., 2001). We therefore generated transgenic worms that expressed a dominant negative variant of UNC-116 (E160A) that is predicted to trap the protein in a rigor state (Klumpp et al., 2003). The rapid movement of GLR-1: :GFP vesicles was eliminated in worms that expressed UNC-116(E160A) solely in AVA (Figure 4A–4D). We also failed to observe vesicle movement in transgenic worms where UNC-116 was knocked down specifically in AVA using double-stranded RNAi [*unc-116(RNAi)*] (Figure 4A–4D). We could rescue the defective transport of GLR-1: :GFP in *unc-116(wy270)* mutants by specifically expressing a wild-type *unc-116* transgene in AVA (Figure 4A–4D), indicating a cell-autonomous role for UNC-116-mediated transport of GLR-1.

Kinesin-1 motors are tetrameric proteins composed of two heavy chains (UNC-116) and two light chains. In *C. elegans*, the genes encoding the kinesin light chains (*klc-1* and *klc-2*) are broadly expressed (Sakamoto et al., 2005) (www.wormbase.org). Light chains regulate the binding of cargo to the motor and are involved in the recruitment of the motor to microtubule tracks (Hirokawa et al., 2010). To determine whether KLC-1 or KLC-2 light chains regulate GLR-1 transport, we examined GLR-1: :GFP movement in light chain mutants. Transport was severely disrupted in *klc-2*, but not *klc-1* mutants (Figure 4E and 4F), indicating that GLR-1 transport is dependent on a specific isoform of kinesin-1.

To determine the subcellular distribution of UNC-116, we coexpressed fluorescently labeled UNC-116: :mCherry with GLR-1: :GFP in the AVA neurons. While UNC-116 was detected throughout the processes, we noted that it appeared to accumulate at synapses (Figure 4G). We also simultaneously measured the movement of GLR-1: :mCherry and UNC-116: :GFP using two-color streaming confocal movies. As predicted for kinesin-driven transport of GLR-1, we found that the two signals colocalized in a subset of transport events, including retrograde movement towards the cell body (Figure 4H).

Kinesin-1 motors direct movement towards the plus-end of microtubules, which are typically oriented plus-end out, i.e., towards the distal ends of axonal processes (Stepanova et al., 2003). Because we observed bidirectional movement of GLR-1: :GFP, we asked whether microtubules in AVA were of mixed polarity, similar to what has been observed in *Drosophila* dendrites (Stone et al., 2008; Zheng et al., 2008). Examination of microtubule growth dynamics in transgenic worms that expressed the microtubule end-binding protein EBP-2 (Stepanova et al., 2003; Zheng et al., 2008) fused to GFP revealed both plus-end out and minus-end out microtubules, consistent with bidirectional transport by UNC-116/KIF5 (Figure S4C and S4D). Additionally, we did not find that microtubule orientation or dynamics were disrupted in *unc-116* mutants (Figure S4C and S4D), indicating that the disrupted transport of GLR-1 in *unc-116* mutants was not an indirect effect of altered microtubules.

GLR-1 removal from synapses is reduced in *unc-116* mutants

Although GLR-1 transport was severely disrupted in *unc-116* mutants, we still observed accumulations of GLR-1: :GFP in the proximal AVA processes (Figure 5A). Surprisingly, the average fluorescence intensity of synaptic puncta was considerably increased in *unc-116* mutants compared to wild type (Figure 5A and 5B) and with the same allelic dependence we observed for GLR-1 transport (Figure 4). The increased fluorescence in *unc-116* mutants was not secondary to possible presynaptic defects as we found that the intensity of synaptic GLR-1: :GFP puncta was rescued by the selective expression of UNC-116 in AVA (Figure 5A and 5B).

To determine whether *C. elegans* kinesin-1 could also mediate the transport of vertebrate AMPARs, we expressed the vertebrate AMPAR subunit GluA1 fused to GFP in the AVA neurons. GluA1: :GFP is functional and localized to puncta in the neural processes (Figure S5) (Brockie et al., 2013). Similar to what we observed for GLR-1, transport of GluA1: :GFP was significantly impaired and the receptor accumulated at synaptic puncta in *unc-116* mutants compared to wild-type worms (Figure S5).

We reasoned that the accumulations of GLR-1 in *unc-116* mutants might be secondary to defective removal of synaptic receptors. To test this hypothesis, we photoconverted GLR-1: :Dendra 2 at single synapses (Figure 5C). Following photoconversion, the red fluorescence decreased in wild-type worms with approximately 25% remaining 4 hours after conversion (Figure 5D). In contrast, decay was significantly reduced in *unc-116* mutants with the slowest decay observed in *unc-116(RNAi)*. These results indicate that the removal of synaptic receptors is dependent on UNC-116/KIF5, consistent with the observed increase in synaptic GLR-1: :GFP in *unc-116* mutants.

UNC-116/KIF5 is required for the delivery of synaptic GLR-1

In contrast to the increased GLR-1: :GFP fluorescence in the proximal processes of *unc-116* mutants, fluorescence intensity in distal regions of the AVA processes was decreased compared to that in wild-type worms (Figure 5E and 5F, and Figure S6A). This finding, along with our analysis of vesicle stoppage and insertion (Figure 2), suggests that UNC-116/KIF5 is also required for the normal delivery of GLR-1 to synapses. Because diffusion depends on the square root of time, it is inefficient over long distances. Although the young adult worms we study are approximately 96 hours old, the number of synaptic GLR-1 receptors at more distal synapses was reduced in the absence of UNC-116/KIF5-mediated transport (Figure 5E). Assuming that the diffusion constant for receptors in the cell membrane is approximately 0.1 $\mu m^2/s$ (Earnshaw and Bressloff, 2008), we estimate that 96 hours is sufficient time for GLR-1 receptors to diffuse to proximal synapses, but not long enough to reach distal synapses. In support of this, line scans of GLR-1: :GFP fluorescence in *unc-116(RNAi)*, and *unc-116(rh24)* mutants revealed dramatically reduced fluorescence in the distal processes when compared to fluorescence in more proximal regions, a pattern consistent with a diffusion-driven process (Figure S6A). We considered whether other motors might contribute to GLR-1 transport earlier in development thereby confounding the interpretation of our line-scan analysis. However, in larval L2 stage *unc-116* mutants (Figure S6B and S6C), we found defects in GLR-1 puncta and transport similar to those of adult *unc-116* mutants (Figures 4 and 5).

To directly test the contribution of motor-mediated delivery of GLR-1 to synapses, we photobleached the entire distal half of the AVA processes and monitored the return of GFP fluorescence in three regions within the photobleached area (Figure 5G). Four hours after photobleaching, we observed significant fluorescence recovery in all distal regions in wild-type worms (67.5 ± 8.2%, n=4) (Figure 5H and 5I). In contrast, essentially no recovery was

observed in *unc-116(RNAi)* mutants (3.5 ± 1.4%, n=4, p<0.01). Thus, in *unc-116* mutants, receptors diffused out of the cell body to proximal synapses where they accumulated secondary to defective removal.

Blocking protein synthesis does not appreciably alter delivery of GLR-1 to synapses

While our data indicate that UNC-116/KIF5 has a critical role in receptor removal and delivery, other mechanisms, such as local synthesis of GLR-1, might also contribute to the number of synaptic receptors. For example, UNC-116/KIF5 might transport mRNA encoding GLR-1 to distal synapses, thus complicating the interpretation of our photobleaching studies. To evaluate the role of local GLR-1 synthesis, we blocked protein synthesis by acutely treating worms with the drug cycloheximide (CHX) for six hours (Jensen et al., 2012; Kourtis and Tavernarakis, 2009). We reasoned that if local synthesis of GLR-1 contributed to new synaptic receptors, treatment with CHX should significantly slow fluorescence recovery following photobleaching of GLR-1: :GFP. Although CHX blocked new protein synthesis (Figure S7A), it did not disrupt existing GLR-1: :GFP puncta or motor-mediated transport of GLR-1 (Figures S7B and S7C). Importantly, we did not observe an appreciable difference in the recovery of CHX-treated and untreated wild-type worms (Figure S7C). These data indicate that the repopulation of synaptic GLR-1 during the four hours following photobleaching is primarily dependent on motor-driven transport.

The intensity of GLR-1: :GFP puncta is decreased in *klp-4* mutants

Although we did not observe any transport in *unc-116(RNAi)* worms, it is possible that additional kinesin motors might contribute to GLR-1 transport. In contrast to the accumulation of receptors in *unc-116* mutants, we observed a decrease in synaptic GLR-1: :GFP fluorescence in mutants that lacked the Kinesin-3 motor KLP-4 (Figure S8A and S8B), which is consistent with an earlier report on *klp-4* mutants (Monteiro et al., 2012). Further analysis revealed that GLR-1: :GFP puncta intensities were similarly diminished in *klp-4* mutants and *unc-116; klp-4* double mutants, indicating that *klp-4* is epistatic to *unc-116* and suggesting that KLP-4 functions upstream of UNC-116/KIF5-mediated transport of GLR-1. While GLR-1: :GFP synaptic puncta were smaller in *klp-4* mutants, analysis of the kymographs revealed apparently normal transport of vesicles in the AVA processes compared to the severely disrupted transport in *unc-116* mutants and *unc-116; klp-4* double mutants (Figure S8C and S8D). Additionally, we did not detect any apparent difference in the intensity of GLR-1: :GFP transport vesicles in *klp-4* mutants (data not shown). Our data suggest that KLP-4 motors likely act in the cell body to regulate the number of exported GLR-1, but they apparently do not have a direct role in the long-range transport of GLR-1 vesicles in neuronal processes.

GLR-1 surface expression is increased in *unc-116* mutants

In *unc-116* mutants, the intensity of synaptic GLR-1: :GFP fluorescence in the proximal processes was increased compared to wild type. However, two populations of GLR-1 contribute to this fluorescent signal, i.e., receptors at the surface and receptors localized to subcellular compartments. To determine whether the number of surface receptors was modified by motor transport, we examined the relative levels of GLR-1 tagged with superecliptic pHluorin (SEP: :GLR-1) in wild type and *unc-116* mutants. Interestingly, we found that surface SEP: :GLR-1 fluorescence was considerably increased following RNAi knockdown of UNC-116 in AVA compared to that observed in wild type (Figure 6A and 6B).

Since both the total pool of GLR-1 (GLR-1: :GFP) and surface-expressed GLR-1 (SEP: :GLR-1) were increased in *unc-116* mutants, we next asked whether the ratio of surface to total receptors was modified. We examined SEP: :mCherry: :GLR-1 at synapses

and found that the ratio of surface to total receptors was considerably increased in *unc-116* mutants compared to wild type (Figure 6C and 6D). This increase was similar to that in transgenic worms that expressed SEP::mCherry::GLR-1(4KR) – an ubiquitination-defective variant of GLR-1 that is predicted to increase the number of cell-surface synaptic receptors (Burbea et al., 2002; Grunwald et al., 2004).

Together, our data suggest a model in which GLR-1 receptors in *unc-116* mutants diffuse within the membrane to synaptic sites where they preferentially remain at the surface. The altered ratio of surface to internal receptors might reflect a decreased rate of local receptor endocytosis, or an increased rate of receptor recycling to the cell surface. To distinguish between these possibilities, we photobleached SEP::mCherry::GLR-1 in either transgenic wild-type worms or *unc-116* mutants and quantified the rate of GLR-1 surface insertion by the appearance of SEP fluorescence. In transgenic wild-type worms that expressed either SEP::mCherry::GLR-1 or SEP::mCherry::GLR-1(4KR), we were able to detect insertion events, with GLR-1(4KR) having a higher rate of insertion (Figure 6E and 6F). In contrast, we did not observe any insertion events in *unc-116* mutants (Figure 6E and 6F). The observed defects in receptor removal and recycling in *unc-116* mutants suggest that UNC-116/KIF5 might also be required for the delivery of critical endosomal machinery.

Glutamate-gated currents are decreased in *unc-116* mutants

Based on our finding that loss of UNC-116/KIF5 function is associated with an increase in GLR-1::GFP surface expression, we predicted that voltage-clamp recordings from the proximal processes of AVA in these transgenic *unc-116* mutants worms would reveal an increase in glutamate-gated currents. Instead, we found that glutamate-gated currents in AVA were significantly decreased. This defect was cell autonomous as we could rescue the current by specifically expressing UNC-116 in the AVA neurons (Figure 7A and 7B). This decrease in current was independent of the GLR-1::GFP transgene as we found similar decreases in current when recording from *unc-116(RNAi)* or *unc-116(wy270)* mutants that did not express the transgene (Figures S9). In contrast, the increased surface expression of GLR-1(4KR) resulted in larger glutamate-gated currents compared to wild-type GLR-1 (Figure 7A and 7B). However, current amplitudes in transgenic *unc-116(RNAi)* mutants that expressed either GLR-1::GFP or GLR-1(4KR)::GFP were indistinguishable and dramatically reduced compared to wild-type transgenic worms (Figure 7A and 7B). Thus, although surface GLR-1 was increased in *unc-116* mutants, glutamate-gated currents were paradoxically decreased.

Because of the diminished GLR-1-mediated currents in *unc-116* mutants, we asked whether a known GLR-1 mediated behavior was also disrupted. Similar to *glr-1* mutants (Hart et al., 1995; Maricq et al., 1995), we found that *unc-116(e2310)* mutants were defective in their avoidance response to tactile stimulation of the nose (Figure 7C). We could partially rescue this response in transgenic *unc-116* mutants that expressed a wild-type *unc-116* transgene under control of the *glr-1* promoter (*Pglr-1::unc-116*).

Overexpressing the AMPAR signaling complex restored current in *unc-116* mutants

We speculated that the diminished glutamate-gated current in *unc-116* mutants, despite increased GLR-1 surface expression, was secondary to defects in the GLR-1 signaling complex. Perhaps the delivery of a key postsynaptic component was limited in the absence of motor function. To test this possibility, we measured glutamate-gated currents in transgenic wild-type worms and *unc-116* mutants that expressed GLR-1::GFP either with or without a second multi-transgene array that encoded all of the additional known components of the GLR-1 signaling complex (GLR-2, SOL-1, SOL-2 and STG-2) (Brockie et al., 2001; Mellem et al., 2002; Walker et al., 2006; Wang et al., 2012; Wang et al., 2008; Zheng et al.,

2006; Zheng et al., 2004). Remarkably, overexpressing the signaling complex was sufficient to restore glutamate-gated currents in transgenic *unc-116* mutants (Figure 7D and 7E). Furthermore, currents in *unc-116* mutants were several-fold larger than those observed in transgenic wild-type worms. Presumably, this increase in *unc-116* mutants was secondary to a change in the composition of the GLR-1 signaling complex in addition to the observed increase in surface expression of GLR-1 (Figure 7). In contrast, the number of surface GLR-1 signaling complexes is well-regulated in wild-type worms, and therefore currents did not appreciably change with overexpression of the signaling complex (Figure 7D and 7E). These results indicate that in the absence of overexpression, the levels of one or more components of the GLR-1 signaling complex are diminished in *unc-116* mutants, thus limiting the number of functional receptors.

To determine the missing component(s) of GLR-1 signaling complexes in *unc-116* mutants, we used confocal microscopy to evaluate the distribution of the components in the proximal processes of AVA. Similar to GLR-1, we found increased synaptic accumulations of STG-2, SOL-1 and SOL-2 in *unc-116* mutants compared to wild type (Figure 8A and 8B). In contrast, we found the opposite pattern with GLR-2 and observed a considerable decrease in GLR-2 levels in *unc-116* mutants compared to wild type. (Figure 8A and 8B).

These results suggest that the decrease in glutamate-gated current in *unc-116* mutants was secondary to decreased GLR-2 at synapses. Thus, although GLR-1 receptors accumulate at synapses in *unc-116* mutants, synaptic transmission is impaired because the signaling complex lacks the GLR-2 subunit. In support of this conclusion, in a previous study we found that currents in *glr-2* mutants are decreased in amplitude (Mellem et al., 2002).

One possible explanation for the decreased synaptic GLR-2 in *unc-116* mutants is that in the absence of UNC-116/KIF5-mediated transport, GLR-2-containing receptors are diverted to the lysosome for degradation. Consistent with this possibility, we found that the levels of GLR-2 were greatly reduced in the AVA cell bodies in *unc-116* mutants (Figure 8C and 8D). To evaluate the contribution of possible lysosomal degradation, we examined GLR-2 levels in transgenic worms that expressed a dominant-negative (DN) variant of the AAA-type ATPase, VPS-4, that mediates sorting of cargo from endosomes to the multivesicular body (Babst et al., 2002; Chun et al., 2008). In *vps-4(DN); unc-116* double mutants, we found that the GFP: :GLR-2 signal was significantly increased compared to that in *unc-116* single mutants (Figure 8C and 8D). This result is consistent with increased lysosomal-mediated degradation of GLR-2 in *unc-116* mutants.

Heat-shock expression of UNC-116/KIF5 in adult mutants rescued synaptic defects

We next asked whether the GLR-1 transport and synaptic defects in *unc-116* mutants could be rescued in adult worms by expressing UNC-116/KIF5 specifically at the adult stage. Using a heat-shock promoter to induce expression of a wild-type *unc-116* transgene in adult *unc-116* mutants, we found that both the number of GLR-1: :GFP transport events and synaptic puncta intensity were restored to near wild-type levels (Figure 9A–9C). Consistent with the normalization of synaptic puncta intensity following heat shock, we also found that glutamate-gated currents were significantly increased (Figure 9D and 9E). These data demonstrate that transport and redistribution of GLR-1 in the adult nervous system is ongoing and dependent on UNC-116/KIF5.

Discussion

We have demonstrated that kinesin-1 (UNC-116/KIF5) mediates the delivery, removal and redistribution of GLR-1 AMPARs in *C. elegans* neurons, and that this motor-driven transport is of critical importance for synaptic function in the adult nervous system. Our *in*

vivo studies have also shed new light on the relative roles of diffusion, local synthesis and motor-dependent transport in the establishment and maintenance of glutamatergic synapses. Defective motor-driven transport of AMPARs leads to an accumulation of dysfunctional AMPARs at synapses that lack the GLR-2 subunit; however, even after chronic loss of motor function, the synaptic defects could be corrected by transient expression of functional kinesin-1 motors.

UNC-116/KIF5 mediates the delivery, removal and redistribution of synaptic AMPARs

Streaming movies of GLR-1::GFP revealed bidirectional motor-driven transport of AMPARs along the AVA processes that was dependent on UNC-116/KIF5. Although diffusion of GLR-1 in *unc-116* mutants is sufficient to populate proximal synaptic sites over a developmental time course of four days, receptors do not reach distal synapses, i.e., those greater than ~600 μm from the cell body. In contrast, motor-driven transport allows for the rapid delivery of receptors along the entire length of the processes. Thus, after photobleaching synaptic GLR-1::GFP, motor-dependent delivery of new receptors occurred within minutes and was the dominant process in the recovery of the fluorescent signal. Because neither diffusion nor local translation appeared to significantly contribute to fluorescence recovery in this time period, we conclude that delivery of new receptors is primarily dependent on kinesin-mediated transport. Although AMPARs labeled with quantum dots in cultured neurons have been observed moving between neighboring synapses by diffusing in the cell membrane (Ehlers et al., 2007), we now show that AMPARs are actively redistributed to distant synapses. This indicates that receptors are not simply destined for a single synapse, but rather can be utilized at multiple synapses.

GLR-1-mediated currents were reduced in *unc-116* mutants even though levels of the GLR-1 subunit and auxiliary proteins were increased. In *unc-116* mutants, we found an increased number of GLR-1 receptors at the surface suggesting defective endocytosis of GLR-1. Thus, kinesin-1 might deliver endosomal machinery to synapses that are required for the removal of GLR-1 receptors. In addition, we found that GLR-2 containing AMPARs appear to be more dependent on kinesin-mediated transport. Because the majority of the glutamate-gated current in wild-type worms is mediated by GLR-1/GLR-2 heteromers (Mellem et al., 2002), the current is reduced in *unc-116* mutants even though surface expression of GLR-1 is increased. Alternatively, if GLR-2 is required for the endocytosis of GLR-1/GLR-2 heteromers, then the increased synaptic GLR-1 in *unc-116* mutants might be secondary to the relative lack of synaptic GLR-2. However, the surface to internal ratio of SEP::mCherry::GLR-1 in *glr-2* mutants was not appreciably different from wild type (data not shown).

Of particular interest was our observation that glutamate-gated currents in *unc-116* mutants that overexpressed all components of the signaling complex were far larger than those measured in either *unc-116* mutants or wild-type worms. In contrast, current magnitudes in wild-type worms either with or without overexpression of all components of the signaling complex were identical. These findings indicate that the balance between kinesin-dependent delivery and removal of AMPARs is critical for regulating synaptic strength, and that regulation of these transport processes could provide an additional mechanism for the homeostatic scaling of synaptic signaling (Davis, 2006; Goold and Nicoll, 2010; Tatavarty et al., 2013; Turrigiano, 2008). A recent paper from the Nicoll and Roche groups addressed distance-dependent scaling, and demonstrated increased surface levels of AMPARs in distal synapses compared to proximal synapses (Shipman et al., 2013). Although we have not directly addressed this question, we found that the SEP::mCherry::GLR-1 ratio varied along the length of the AVA processes. Thus, the percentage of GLR-1 at the surface increased proximally to distally (data not shown).

UNC-116/KIF5 transport: Implications for synaptic plasticity

How the strength of synaptic communication between neurons is modified by experience-dependent neural activity is still an open question. The synaptic tag and capture (STC) hypothesis posits that synaptic activity leads to molecular changes that "tag" a synapse to enhance the probability of capturing plasticity-related proteins (PRPs) required for changes in synaptic strength. Thus, early-LTP (long term potentiation) of a synapse leads to local molecular changes (synaptic tagging) and the local synthesis of diffusible PRPs that are then captured by the tagged synapse (Redondo and Morris, 2011).

Our experiments suggest a new model of synaptic capture where activity-dependent synaptic tagging increases the probability of motor-dependent delivery of AMPARs. We found that receptor movement is highly dynamic in the AVA neurons, which have a large pool of motor-transported receptors. This ensures that any given synapse is only a few seconds removed from a motor carrying AMPARs allowing for rapid, activity dependent changes in synaptic AMPARs that are independent of new protein synthesis. We suggest that synaptic tagging and motor-dependent delivery can also contribute to longer timescale, protein synthesis-dependent plasticity. Protein synthesis associated with late-LTP might fortify the synaptic tag, thus maintaining the probability of motor-dependent receptor delivery. In this process, the tagged synapse can become self-sustaining as long as motor-transport is unimpaired.

Our studies raise several important questions. First, what are the local signals for kinesin-mediated delivery and removal of synaptic AMPARs? We can imagine that these processes are regulated by synaptic activity and thus, could serve as a mechanism for local strengthening or weakening of synapses, i.e., LTP or LTD (long term depression). Although the nature of the synaptic tag has not yet been identified (Redondo and Morris, 2011), we expect that genetic analysis in *C. elegans* will distinguish between possible mechanisms for synaptic tagging, including local modification of microtubules, recruitment of actin for hand-off to myosin-class motors, local increases in intracellular Ca^{2+} and local depletion of ATP causing stalling of motors at synapses (Guillaud et al., 2008; Kapitein et al., 2013; Maas et al., 2009; Newby and Bressloff, 2010; Newby and Bressloff, 2009). Second, what distinguishes GLR-1 homomers from GLR-1/GLR-2 heteromers with respect to motor-mediated transport? In the absence of kinesin-1, heteromers are selectively degraded suggesting the involvement of a possible GLR-2 specific cargo adaptor protein. Third, how are the other components of the GLR-1 signaling complex delivered and removed from synapses? Fourth, what are the relevant cargo adaptors? An early report implicated the GRIP1 scaffolding protein in kinesindependent trafficking (Setou et al., 2002), but conditional knockout of GRIP proteins did not appear to disrupt the steady state trafficking or endocytosis of AMPARs (Mao et al., 2010). Finally, while our results clearly demonstrate that UNC-116/KIF5 is required for the long-range transport of GLR-1, we would expect that additional motors such as dynein, other kinesins, or unconventional myosins might contribute to this process, as well as to other aspects of delivery such as switching of transport direction and short-range transport at the synapse.

Altered transport is found in a variety of neurological disorders and presumably contributes to the disrupted synaptic function that is evident at all stages of diseases such as Alzheimer's (Hirokawa et al., 2010; Ittner and Gotz, 2011; Stokin and Goldstein, 2006). Our results demonstrate a critical role of kinesin in the establishment and maintenance of glutamatergic synapses, and suggest that defective synaptic signaling secondary to altered transport might be restored by repairing the underlying transport defect.

Experimental Procedures

Strains and Genetics

All *C. elegans* strains were raised under standard conditions on the *E. coli* strain OP50 at 20 °C unless otherwise noted. Wild-type worms were the Bristol N2 strain. Transgenic worms were generated by gonadal microinjection of *lin-15(n765ts)* mutants, wild type or appropriate mutant worms. Transgenic animals were selected by rescue of the *lin-15(n765ts)* mutant phenotype or expression of a fluorescent coinjection marker. Plasmids, transgenic arrays and strains are described in Supplemental Experimental Procedures. All fluorescently labeled proteins were found to be functional in transgenic rescue experiments of the mutant phenotype.

Spinning Disk Confocal Imaging

One-day-old adult worms were mounted on 10% agarose pads with 1 μl of 30 mM muscimol unless otherwise indicated. Images were acquired using a spinning disk confocal. Transport images were acquired by taking a streaming movie in a single Z-plane with 100 ms exposure time unless otherwise stated. GLR-1 was tagged with GFP, SEP, mCherry, or SEP::mCherry either at the N-terminus (SEP::GLR-1 and SEP::mCherry::GLR-1), or near the C-terminus (GLR-1::GFP, GLR-1::mCherry) as described previously (Rongo et al., 1998). The trajectory of moving GLR-1::GFP particles was quantified on kymographs in MetaMorph 7.7.7 (Molecular Devices) or Matlab 2012a (MathWorks) and analyzed with a custom written Matlab script to yield velocity, run length, flux, pause time and stopping/insertion location. Fluorescence intensities of synaptic puncta were measured using a linescan measurement in MetaMorph and analyzed with a custom written MATLAB script (based on http://terpconnect.umd.edu/~toh/spectrum/PeakFindingandMeasurement.htm). All other image analysis was performed in MetaMorph or ImageJ. A more detailed description of these procedures can be found in Supplemental Experimental Procedures.

Photobleaching, photoconversion and photoactivation

Photobleaching was achieved using an argon laser (Coherent) set to 1.6 W total power output and/or a 561 nm laser (CNI Lasers) set to 600 mW total power output. GLR-1::Dendra2 and GLR-1::PAGFP were photoconverted and photoactivated, respectively, using a 405 nm laser (Coherent) set at 35 mW total power output. Lasers and laser merge module were provided by Spectral Applied Research. Regions of interest for photobleaching, photoconversion and photoactivation were selected using a Mosaic II digital mirror device (Andor) controlled through MetaMorph. After photobleaching the distal region of the processes (Figure 5), the worms were transferred from the agarose pad on a microscope slide to a standard agar dish for 4 hrs where they could move freely and feed. The worms were then transferred back to agarose pads for imaging. For photoconversion and redistribution experiments, worms were mounted on 10% agarose pads with 1.5 μl polystyrene beads (Kim et al., 2013). A detailed description of the quantification and procedures for FRAP, photoconversion and redistribution experiments can be found in Supplemental Experimental Procedures.

Na-azide and nocodazole treatments

For Na-azide treatment, worms were incubated in 40 mM Na-azide in M9 buffer on agar pads for 20 min at room temperature before imaging GLR-1 transport. For nocodazole treatment, 30 mM nocodazole in DMSO, or DMSO alone as control, was injected into the pseudocoelome of worms 1 hr prior to imaging.

Heat shock treatment

Induction of *Phsp-unc-116-mCherry* expression was achieved by two heat-shock treatments of 1 hr each at 33° C separated by 12 hrs at room temperature. Worms were imaged 4 hrs following the second heat shock. For electrophysiology experiments, currents were recorded in worms with high expression of UNC-116::mCherry in AVA 12 hrs after heat shock.

Electrophysiology

Electrophysiological recordings were performed blind to genotype and treatment using previously described voltage-clamp techniques (Mellem et al., 2002). With the exception of Figure S9, all worms expressed either GLR-1::GFP or GLR-1(4KR)::GFP in AVA.

Behavioral Analysis

Nose touch response assays were preformed as described in (Mellem et al, 2002). All assays were preformed blind to genotype.

Statistical analysis

The results were analyzed using an unpaired Student's *T*-test.

Supplementary Material

Refer to Web version on PubMed Central for supplementary material.

Acknowledgments

We thank members of the Maricq laboratory for comments on the manuscript, Aleksander Maricq for assistance with data analysis and Linda Hauth for generating transgenic strains. We thank Josh Kaplan, Kang Shen and Yishi Jin for providing worm strains. Some strains were provided by the *Caenorhabditis* Genetics Center (CGC), which is funded by NIH Office of Research Infrastructure Programs (P40 OD010440). This research was made possible by support from NIH Grant NS35812 (A.V.M.), a Human Frontier Science Program grant (A.V.M.), and by postdoctoral fellowships from the Swiss National Science Foundation (F.J.H.).

References

Adesnik H, Nicoll RA, England PM. Photoinactivation of native AMPA receptors reveals their real-time trafficking. Neuron. 2005; 48:977–985. [PubMed: 16364901]

Babst M, Katzmann DJ, Snyder WB, Wendland B, Emr SD. Endosome-associated complex, ESCRT-II, recruits transport machinery for protein sorting at the multivesicular body. Developmental cell. 2002; 3:283–289. [PubMed: 12194858]

Bowler MW, Montgomery MG, Leslie AG, Walker JE. How azide inhibits ATP hydrolysis by the F-ATPases. Proc Natl Acad Sci U S A. 2006; 103:8646–8649. [PubMed: 16728506]

Brockie PJ, Jensen M, Mellem JE, Jensen E, Yamasaki T, Wang R, Maxfield D, Thacker C, Hoerndli F, Dunn PJ, et al. Cornichons Control ER Export of AMPA Receptors to Regulate Synaptic Excitability. Neuron. 2013; 80:129–142. [PubMed: 24094107]

Brockie PJ, Mellem JE, Hills T, Madsen DM, Maricq AV. The C. elegans glutamate receptor subunit NMR-1 is required for slow NMDA-activated currents that regulate reversal frequency during locomotion. Neuron. 2001; 31:617–630. [PubMed: 11545720]

Burbea M, Dreier L, Dittman JS, Grunwald ME, Kaplan JM. Ubiquitin and AP180 regulate the abundance of GLR-1 glutamate receptors at postsynaptic elements in C. elegans. Neuron. 2002; 35:107–120. [PubMed: 12123612]

Byrd DT, Kawasaki M, Walcoff M, Hisamoto N, Matsumoto K, Jin Y. UNC-16, a JNK-signaling scaffold protein, regulates vesicle transport in C. elegans. Neuron. 2001; 32:787–800. [PubMed: 11738026]

Chun DK, McEwen JM, Burbea M, Kaplan JM. UNC-108/Rab2 regulates postendocytic trafficking in Caenorhabditis elegans. Mol Biol Cell. 2008; 19:2682–2695. [PubMed: 18434599]

Davis GW. Homeostatic control of neural activity: from phenomenology to molecular design. Annu Rev Neurosci. 2006; 29:307–323. [PubMed: 16776588]

de Bono M, Maricq AV. Neuronal substrates of complex behaviors in C. elegans. Annu Rev Neurosci. 2005; 28:451–501. [PubMed: 16022603]

Dittman JS, Kaplan JM. Factors regulating the abundance and localization of synaptobrevin in the plasma membrane. Proc Natl Acad Sci U S A. 2006; 103:11399–11404. [PubMed: 16844789]

Earnshaw BA, Bressloff PC. Modeling the role of lateral membrane diffusion in AMPA receptor trafficking along a spiny dendrite. Journal of computational neuroscience. 2008; 25:366–389. [PubMed: 18320299]

Ehlers MD, Heine M, Groc L, Lee MC, Choquet D. Diffusional trapping of GluR1 AMPA receptors by input-specific synaptic activity. Neuron. 2007; 54:447–460. [PubMed: 17481397]

Feinberg EH, Vanhoven MK, Bendesky A, Wang G, Fetter RD, Shen K, Bargmann CI. GFP Reconstitution Across Synaptic Partners (GRASP) defines cell contacts and synapses in living nervous systems. Neuron. 2008; 57:353–363. [PubMed: 18255029]

Glodowski DR, Chen CC, Schaefer H, Grant BD, Rongo C. RAB-10 regulates glutamate receptor recycling in a cholesterol-dependent endocytosis pathway. Mol Biol Cell. 2007; 18:4387–4396. [PubMed: 17761527]

Goold CP, Nicoll RA. Single-cell optogenetic excitation drives homeostatic synaptic depression. Neuron. 2010; 68:512–528. [PubMed: 21040851]

Greger IH, Esteban JA. AMPA receptor biogenesis and trafficking. Curr Opin Neurobiol. 2007; 17:289–297. [PubMed: 17475474]

Grunwald ME, Mellem JE, Strutz N, Maricq AV, Kaplan JM. Clathrin-mediated endocytosis is required for compensatory regulation of GLR-1 glutamate receptors after activity blockade. Proc Natl Acad Sci U S A. 2004; 101:3190–3195. [PubMed: 14981253]

Guillaud L, Wong R, Hirokawa N. Disruption of KIF17-Mint1 interaction by CaMKII-dependent phosphorylation: a molecular model of kinesin-cargo release. Nat Cell Biol. 2008; 10:19–29. [PubMed: 18066053]

Gurskaya NG, Verkhusha VV, Shcheglov AS, Staroverov DB, Chepurnykh TV, Fradkov AF, Lukyanov S, Lukyanov KA. Engineering of a monomeric green-to-red photoactivatable fluorescent protein induced by blue light. Nat Biotechnol. 2006; 24:461–465. [PubMed: 16550175]

Hart AC, Sims S, Kaplan JM. Synaptic code for sensory modalities revealed by C. elegans GLR-1 glutamate receptor. Nature. 1995; 378:82–85. [PubMed: 7477294]

Henley JM, Barker EA, Glebov OO. Routes, destinations and delays: recent advances in AMPA receptor trafficking. Trends Neurosci. 2011; 34:258–268. [PubMed: 21420743]

Hirokawa N, Niwa S, Tanaka Y. Molecular motors in neurons: transport mechanisms and roles in brain function, development, and disease. Neuron. 2010; 68:610–638. [PubMed: 21092854]

Ho VM, Lee JA, Martin KC. The cell biology of synaptic plasticity. Science. 2011; 334:623–628. [PubMed: 22053042]

Ittner LM, Gotz J. Amyloid-beta and tau--a toxic pas de deux in Alzheimer's disease. Nat Rev Neurosci. 2011; 12:65–72. [PubMed: 21193853]

Jackson AC, Nicoll RA. The expanding social network of ionotropic glutamate receptors: TARPs and other transmembrane auxiliary subunits. Neuron. 2011; 70:178–199. [PubMed: 21521608]

Jensen M, Hoerndli FJ, Brockie PJ, Wang R, Johnson E, Maxfield D, Francis MM, Madsen DM, Maricq AV. Wnt signaling regulates acetylcholine receptor translocation and synaptic plasticity in the adult nervous system. Cell. 2012; 149:173–187. [PubMed: 22464329]

Ju W, Morishita W, Tsui J, Gaietta G, Deerinck TJ, Adams SR, Garner CC, Tsien RY, Ellisman MH, Malenka RC. Activity-dependent regulation of dendritic synthesis and trafficking of AMPA receptors. Nat Neurosci. 2004; 7:244–253. [PubMed: 14770185]

Juo P, Harbaugh T, Garriga G, Kaplan JM. CDK-5 regulates the abundance of GLR-1 glutamate receptors in the ventral cord of Caenorhabditis elegans. Mol Biol Cell. 2007; 18:3883–3893. [PubMed: 17671168]

Kapitein LC, van Bergeijk P, Lipka J, Keijzer N, Wulf PS, Katrukha EA, Akhmanova A, Hoogenraad CC. Myosin-V opposes microtubule-based cargo transport and drives directional motility on cortical actin. Curr Biol. 2013; 23:828–834. [PubMed: 23602478]

Kennedy MJ, Ehlers MD. Mechanisms and function of dendritic exocytosis. Neuron. 2011; 69:856–875. [PubMed: 21382547]

Kerchner GA, Nicoll RA. Silent synapses and the emergence of a postsynaptic mechanism for LTP. Nat Rev Neurosci. 2008; 9:813–825. [PubMed: 18854855]

Kessels HW, Malinow R. Synaptic AMPA receptor plasticity and behavior. Neuron. 2009; 61:340–350. [PubMed: 19217372]

Kim CH, Lisman JE. A labile component of AMPA receptor-mediated synaptic transmission is dependent on microtubule motors, actin, and N-ethylmaleimide-sensitive factor. J Neurosci. 2001; 21:4188–4194. [PubMed: 11404404]

Kim E, Sun L, Gabel CV, Fang-Yen C. Long-term imaging of Caenorhabditis elegans using nanoparticle-mediated immobilization. PLoS One. 2013; 8:e53419. [PubMed: 23301069]

Klumpp LM, Brendza KM, Rosenberg JM, Hoenger A, Gilbert SP. Motor domain mutation traps kinesin as a microtubule rigor complex. Biochemistry. 2003; 42:2595–2606. [PubMed: 12614154]

Kourtis N, Tavernarakis N. Cell-specific monitoring of protein synthesis in vivo. PLoS One. 2009; 4:e4547. [PubMed: 19234598]

Maas C, Belgardt D, Lee HK, Heisler FF, Lappe-Siefke C, Magiera MM, van Dijk J, Hausrat TJ, Janke C, Kneussel M. Synaptic activation modifies microtubules underlying transport of postsynaptic cargo. Proc Natl Acad Sci U S A. 2009; 106:8731–8736. [PubMed: 19439658]

Malinow R, Malenka RC. AMPA receptor trafficking and synaptic plasticity. Annu Rev Neurosci. 2002; 25:103–126. [PubMed: 12052905]

Mao L, Takamiya K, Thomas G, Lin DT, Huganir RL. GRIP1 and 2 regulate activity-dependent AMPA receptor recycling via exocyst complex interactions. Proc Natl Acad Sci U S A. 2010; 107:19038–19043. [PubMed: 20956289]

Maricq AV, Peckol E, Driscoll M, Bargmann CI. Mechanosensory signalling in C. elegans mediated by the GLR-1 glutamate receptor. Nature. 1995; 378:78–81. [PubMed: 7477293]

Mellem JE, Brockie PJ, Zheng Y, Madsen DM, Maricq AV. Decoding of Polymodal Sensory Stimuli by Postsynaptic Glutamate Receptors in C. elegans. Neuron. 2002; 36:933–944. [PubMed: 12467596]

Miesenbock G, De Angelis DA, Rothman JE. Visualizing secretion and synaptic transmission with pH-sensitive green fluorescent proteins. Nature. 1998; 394:192–195. [PubMed: 9671304]

Monteiro MI, Ahlawat S, Kowalski JR, Malkin E, Koushika SP, Juo P. The kinesin-3 family motor KLP-4 regulates anterograde trafficking of GLR-1 glutamate receptors in the ventral nerve cord of Caenorhabditis elegans. Mol Biol Cell. 2012; 23:3647–3662. [PubMed: 22855524]

Newby J, Bressloff PC. Local synaptic signaling enhances the stochastic transport of motor-driven cargo in neurons. Physical biology. 2010; 7:036004. [PubMed: 20733246]

Newby JM, Bressloff PC. Directed intermittent search for a hidden target on a dendritic tree. Physical review E, Statistical, nonlinear, and soft matter physics. 2009; 80:021913.

Petrini EM, Lu J, Cognet L, Lounis B, Ehlers MD, Choquet D. Endocytic trafficking and recycling maintain a pool of mobile surface AMPA receptors required for synaptic potentiation. Neuron. 2009; 63:92–105. [PubMed: 19607795]

Redondo RL, Morris RG. Making memories last: the synaptic tagging and capture hypothesis. Nat Rev Neurosci. 2011; 12:17–30. [PubMed: 21170072]

Rongo C, Kaplan JM. CaMKII regulates the density of central glutamatergic synapses in vivo. Nature. 1999; 402:195–199. [PubMed: 10647013]

Rongo C, Whitfield CW, Rodal A, Kim SK, Kaplan JM. LIN-10 is a shared component of the polarized protein localization pathways in neurons and epithelia. Cell. 1998; 94:751–759. [PubMed: 9753322]

Rusakov DA, Savtchenko LP, Zheng K, Henley JM. Shaping the synaptic signal: molecular mobility inside and outside the cleft. Trends Neurosci. 2011

Sakamoto R, Byrd DT, Brown HM, Hisamoto N, Matsumoto K, Jin Y. The Caenorhabditis elegans UNC-14 RUN domain protein binds to the kinesin-1 and UNC-16 complex and regulates synaptic vesicle localization. Mol Biol Cell. 2005; 16:483–496. [PubMed: 15563606]

Setou M, Seog DH, Tanaka Y, Kanai Y, Takei Y, Kawagishi M, Hirokawa N. Glutamate-receptor-interacting protein GRIP1 directly steers kinesin to dendrites. Nature. 2002; 417:83–87. [PubMed: 11986669]

Shepherd JD, Huganir RL. The cell biology of synaptic plasticity: AMPA receptor trafficking. Annu Rev Cell Dev Biol. 2007; 23:613–643. [PubMed: 17506699]

Shipman SL, Herring BE, Suh YH, Roche KW, Nicoll RA. Distance-Dependent Scaling of AMPARs Is Cell-Autonomous and GluA2 Dependent. J Neurosci. 2013; 33:13312–13319. [PubMed: 23946389]

Siddiqui SS. Metazoan motor models: kinesin superfamily in C. elegans. Traffic. 2002; 3:20–28. [PubMed: 11872139]

Stepanova T, Slemmer J, Hoogenraad CC, Lansbergen G, Dortland B, De Zeeuw CI, Grosveld F, van Cappellen G, Akhmanova A, Galjart N. Visualization of microtubule growth in cultured neurons via the use of EB3-GFP (end-binding protein 3-green fluorescent protein). J Neurosci. 2003; 23:2655–2664. [PubMed: 12684451]

Stokin GB, Goldstein LS. Axonal transport and Alzheimer's disease. Annu Rev Biochem. 2006; 75:607–627. [PubMed: 16756504]

Stone MC, Roegiers F, Rolls MM. Microtubules have opposite orientation in axons and dendrites of Drosophila neurons. Mol Biol Cell. 2008; 19:4122–4129. [PubMed: 18667536]

Tatavarty V, Sun Q, Turrigiano GG. How to scale down postsynaptic strength. J Neurosci. 2013; 33:13179–13189. [PubMed: 23926271]

Turrigiano GG. The self-tuning neuron: synaptic scaling of excitatory synapses. Cell. 2008; 135:422–435. [PubMed: 18984155]

Walker CS, Francis MM, Brockie PJ, Madsen DM, Zheng Y, Maricq AV. Conserved SOL-1 proteins regulate ionotropic glutamate receptor desensitization. Proc Natl Acad Sci U S A. 2006; 103:10787–10792. [PubMed: 16818875]

Wang R, Mellem JE, Jensen M, Brockie PJ, Walker CS, Hoerndli FJ, Hauth L, Madsen DM, Maricq AV. The SOL-2/Neto Auxiliary Protein Modulates the Function of AMPA-Subtype Ionotropic Glutamate Receptors. Neuron. 2012; 75:838–850. [PubMed: 22958824]

Wang R, Walker CS, Brockie PJ, Francis MM, Mellem JE, Madsen DM, Maricq AV. Evolutionary conserved role for TARPs in the gating of glutamate receptors and tuning of synaptic function. Neuron. 2008; 59:997–1008. [PubMed: 18817737]

Yudowski GA, Puthenveedu MA, von Zastrow M. Distinct modes of regulated receptor insertion to the somatodendritic plasma membrane. Nat Neurosci. 2006; 9:622–627. [PubMed: 16604070]

Zhang D, Isack NR, Glodowski DR, Liu J, Chen CC, Xu XZ, Grant BD, Rongo C. RAB-6.2 and the retromer regulate glutamate receptor recycling through a retrograde pathway. J Cell Biol. 2012; 196:85–101. [PubMed: 22213799]

Zheng Y, Brockie PJ, Mellem JE, Madsen DM, Walker CS, Francis MM, Maricq AV. SOL-1 is an auxiliary subunit that modulates the gating of GLR-1 glutamate receptors in Caenorhabditis elegans. Proc Natl Acad Sci U S A. 2006; 103:1100–1105. [PubMed: 16418277]

Zheng Y, Mellem JE, Brockie PJ, Madsen DM, Maricq AV. SOL-1 is a CUB-domain protein required for GLR-1 glutamate receptor function in C. elegans. Nature. 2004; 427:451–457. [PubMed: 14749834]

Zheng Y, Wildonger J, Ye B, Zhang Y, Kita A, Younger SH, Zimmerman S, Jan LY, Jan YN. Dynein is required for polarized dendritic transport and uniform microtubule orientation in axons. Nat Cell Biol. 2008; 10:1172–1180. [PubMed: 18758451]

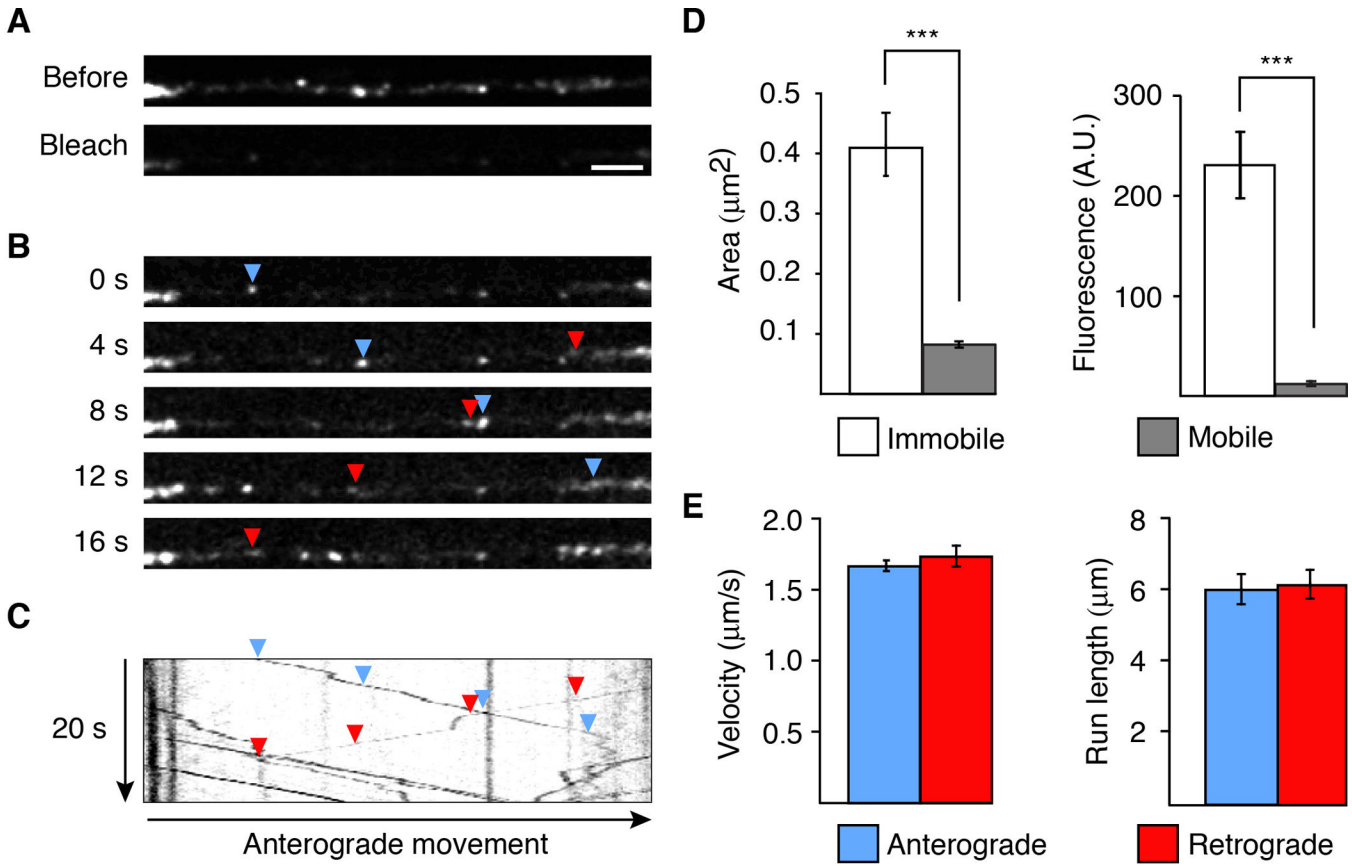

Figure 1. GLR-1: :GFP is transported in both an anterograde and retrograde direction along the AVA processes

(A) Confocal images of GLR-1: :GFP puncta in the proximal AVA processes before (top) and after (bottom) photobleaching. Scale bar represents 2.5 μm. (B) Higher gain images of the region shown in (A) at various time points after photobleaching. The arrowheads indicate anterograde (blue) and retrograde (red) movement. (C) Kymograph showing mobile and immobile GLR-1: :GFP vesicles in the photobleached region shown in (A). (D) Measurement of the area (left) and average total fluorescence (right) of immobile and mobile GLR-1: :GFP, n>100 immobile; n>450 mobile. *** p<0.001. (E) Quantification of the velocity (left) and run length (right) of mobile GLR-1: :GFP vesicles, n>450 vesicles. Error bars indicate standard error of the mean (SEM).

See also Figure S1.

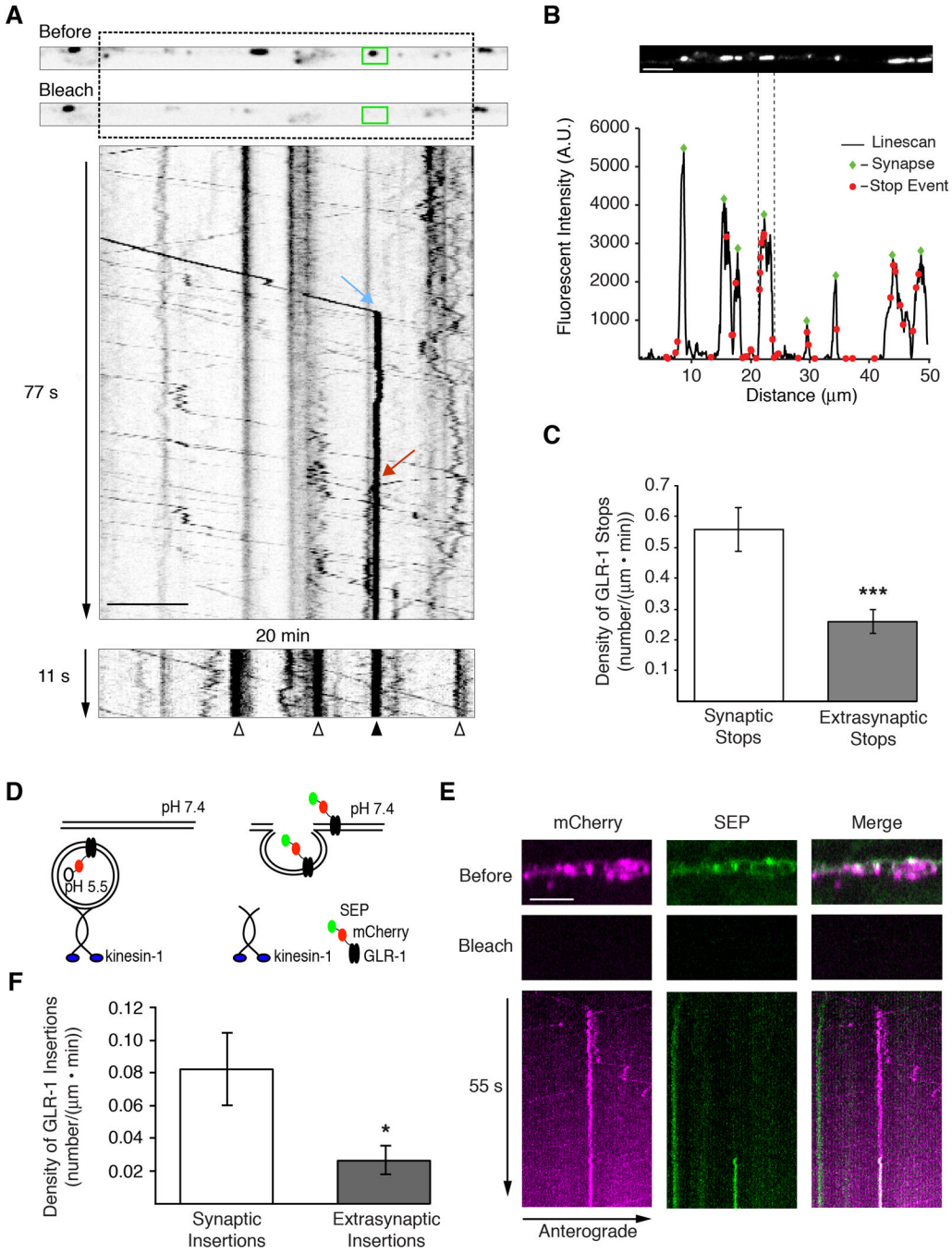

Figure 2. GLR-1 is preferentially delivered to synaptic puncta in the AVA processes

(A) Single plane confocal images before and after photobleaching GLR-1: :GFP in the AVA processes with the corresponding kymograph showing anterograde (blue arrow) and retrograde (red arrow) delivery events to a synaptic puncta (green box). A second kymograph (bottom), taken 20 minutes after the first, shows the stable delivery event from the first kymograph (filled arrowhead), as well as additional delivery events during the interval between the two kymographs (open arrowheads). (B) Confocal image of synaptic GLR-1: :GFP puncta in AVA (top) and the corresponding linescan of fluorescence intensity (bottom). Green diamonds mark the peak fluorescence of synaptic puncta and red dots mark the relative positions of GLR-1: :GFP vesicle stops from a 5 minute movie. (C)

Quantification of GLR-1::GFP vesicle stops in synaptic and extrasynaptic regions, n=7. (D) Cartoon schematic of the double-tagged SEP::mCherry::GLR-1 in transport vesicles and on the cell surface. (E) Simultaneous two-color confocal imaging of SEP::mCherry::GLR-1. Single plane confocal images taken before and after photobleaching (top) and the corresponding kymograph (bottom) showing GLR-1 transport (mCherry signal) and GLR-1 insertion into the membrane (SEP signal). (F) Quantification of GLR-1 insertion events in synaptic and extrasynaptic regions, n=10.
* $p<0.05$, *** $p<0.001$. Scale bars represent 5 μm. Error bars indicate SEM.
See also Figure S2.

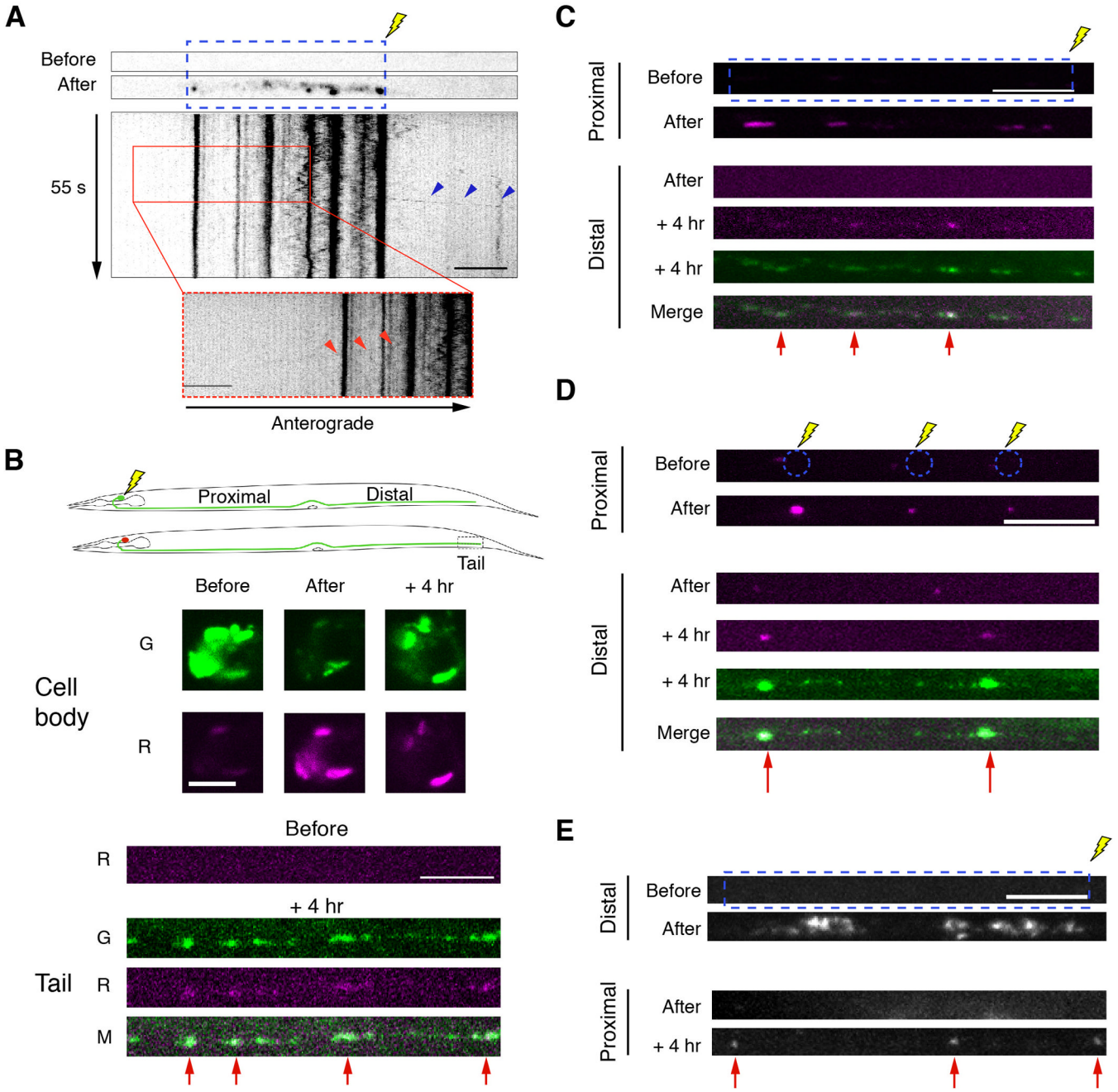

Figure 3. GLR-1 is redistributed between synapses

(A) Photoactivation of GLR-1: :PAGFP expressed in AVA before and after UV photoactivation (blue, dashed box) with the corresponding kymograph. Arrowheads show anterograde (blue arrowheads) and retrograde (inset, red arrowheads) departure of a GLR-1 vesicle from converted synaptic puncta. (B–E) All confocal images were taken before, immediately after, or 4 hours after photoconversion or photoactivation. (B) Schematic of GLR-1: :Dendra2 photoconversion in the cell body (top). Images of GLR-1: :Dendra2 in the cell body and in the distal processes (tail). Red arrowheads highlight synapses that received photoconverted GLR-1: :Dendra2 from the cell body. (C and D) Images of GLR-1: :Dendra2 after photoconversion of total fluorescence (C) or puncta fluorescence only (D) in the

proximal processes (only the red signal is shown). Red arrows indicate the appearance of photoconverted GLR-1: :Dendra2 at distal synapses (red and green signal shown). (E) Images of GLR-1: :PAGFP before and after photoactivation. Red arrows indicate the appearance of photoactivated GLR-1: :PAGFP at proximal synapses.
Scale bars represent 5 μm.
See also Figure S3.

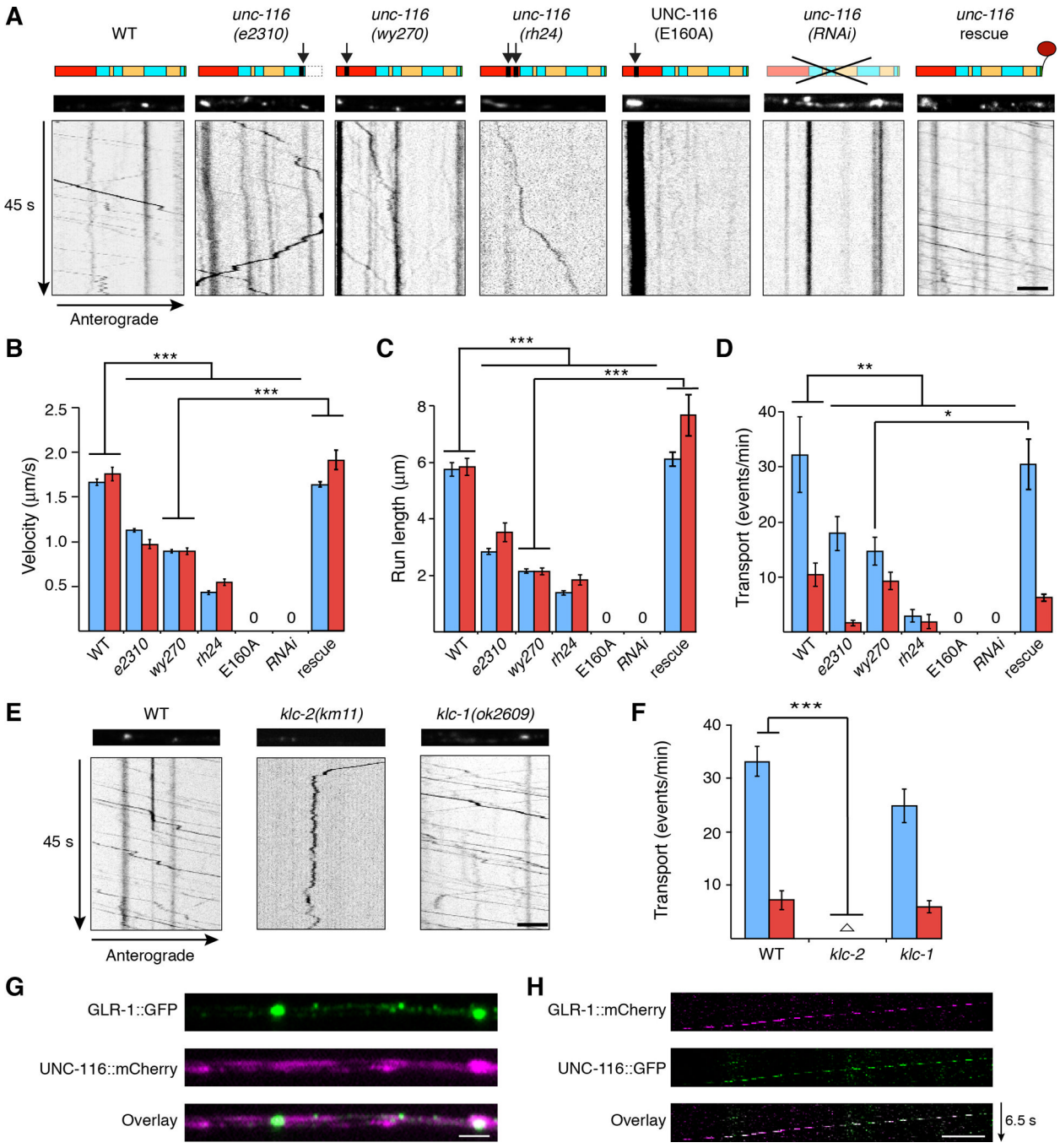

Figure 4. Bidirectional transport of GLR-1 is dependent on UNC-116/KIF5

(A) Schematic of UNC-116/KIF5 (top). Arrows indicate the location of the mutation for each allele (Table S1). Red and yellow boxes represent the motor domain and coiled coil domains, respectively. Confocal images (middle) and kymographs (bottom) of GLR-1: :GFP in the AVA processes. Scale bar represents 2.5 µm. (B–D) Quantification of anterograde (blue) and retrograde (red) vesicle velocity (B), run length (C), and the frequency of transport events (D), n=10 worms. “0” indicates no measurable mobile vesicles. (E) Confocal images (top) and kymographs (bottom) of GLR-1: :GFP in the AVA processes in WT, *klc-2(km11)* and *klc-1(ok2809).* Scale bar represents 5 µm. (F) Quantification of the

frequency of transport events. Empty triangle in *klc-2* represents anterograde = 0.22 events/min and retrograde = 0.17 events/min, n=5. (G) Images of GLR-1: :GFP and UNC-116: :mCherry in the AVA processes of a transgenic worm. Scale bar represents 2 μm. (H) Kymograph showing retrograde co-movement of GLR-1: :mCherry and UNC-116: :GFP in AVA. The breaks in fluorescence are secondary to limited streaming capacity. Scale bar represents 2.5 μm.

* $p<0.05$, ** $p<0.01$, *** $p<0.001$. Error bars indicate SEM.

See also Figures S3, S4 and S5.

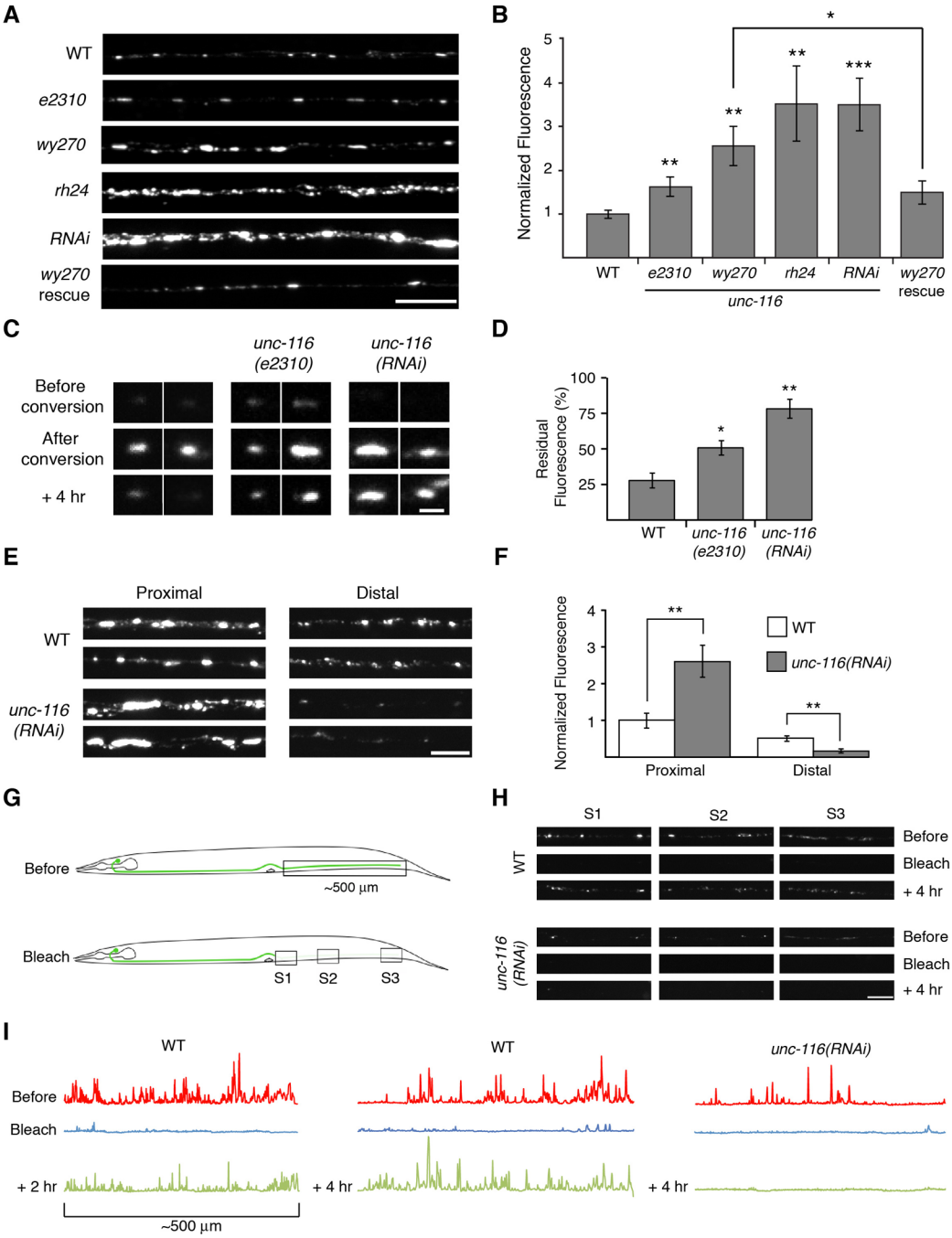

Figure 5. Delivery and removal of synaptic GLR-1 is mediated by UNC-116/KIF5

(A) Confocal images of GLR-1: :GFP puncta in the proximal region of the AVA processes in various transgenic worms. (B) Quantification of GLR-1: :GFP synaptic puncta fluorescence normalized to WT. For all genotypes, n≥10 worms. (C) Confocal images of GLR-1: :Dendra2 synaptic puncta (red signal only) before and after photoconversion. Scale bar represents 1 µm. (D) Quantification of the red signal remaining 4 hours after photoconversion, n=15 puncta per genotype. (E and F) Images (E) and quantification (F) of synaptic GLR-1: :GFP puncta in AVA normalized to the proximal region of WT, n=10 worms. Scale bar represents 5 µm. (G) Cartoon schematic of the distal photobleach experiment. (H) GLR-1: :GFP images before, immediately after, and 4 hours after

photobleaching in the regions indicated in (G). Scale bar represents 5 μm. (I) Linescans of GLR-1: :GFP fluorescence intensity in the distal half of AVA before and after photobleaching.
* $p<0.05$, ** $p<0.01$, *** $p<0.001$. Error bars indicate SEM.
See also Figures S4, S5, S6, S7 and S8.

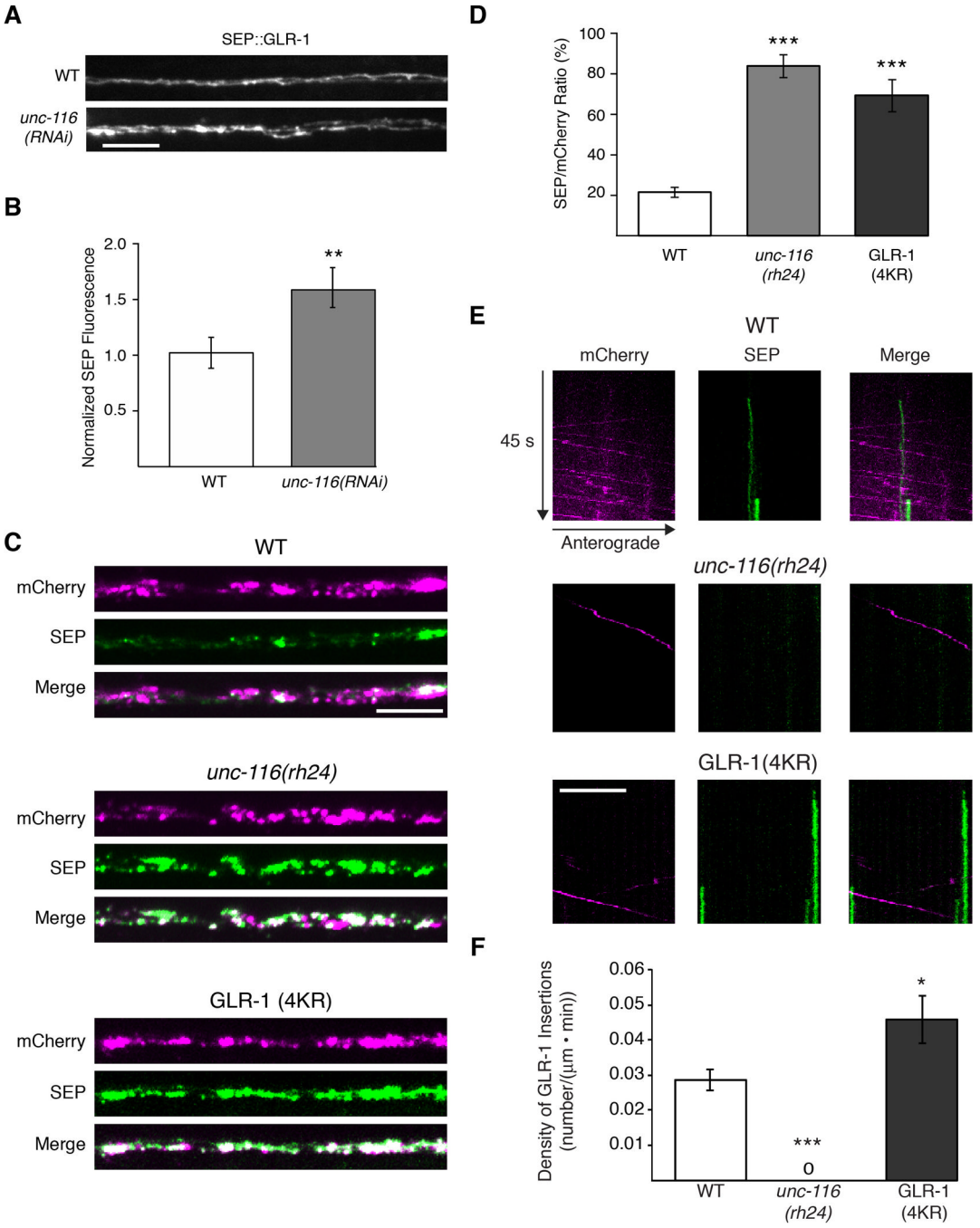

Figure 6. Surface expression of GLR-1 is increased in *unc-116* mutants

(A and B) Images of SEP::GLR-1 fluorescence (A) and quantification (B) of total fluorescence intensity normalized to WT, n=10 worms. (C) Confocal images of SEP::mCherry::GLR-1 and SEP::mCherry::GLR-1(4KR). (D) Ratio quantification of total synaptic SEP and mCherry signals from SEP::mCherry::GLR-1 in WT and *unc-116* mutants, and SEP::mCherry::GLR-1(4KR). For all genotypes, n>15 worms. (E) Kymographs from simultaneous two-color streaming confocal movies of SEP::mCherry::GLR-1 in WT and *unc-116(rh24)*, and SEP::mCherry::GLR-1(4KR). (F)

Quantification of the overall insertion events. “0” indicates no measurable insertion events. For all genotypes, n>15 worms.
Scale bars represent 5μm. * p<0.05, ** p<0.01, *** p<0.001. Error bars indicate SEM.

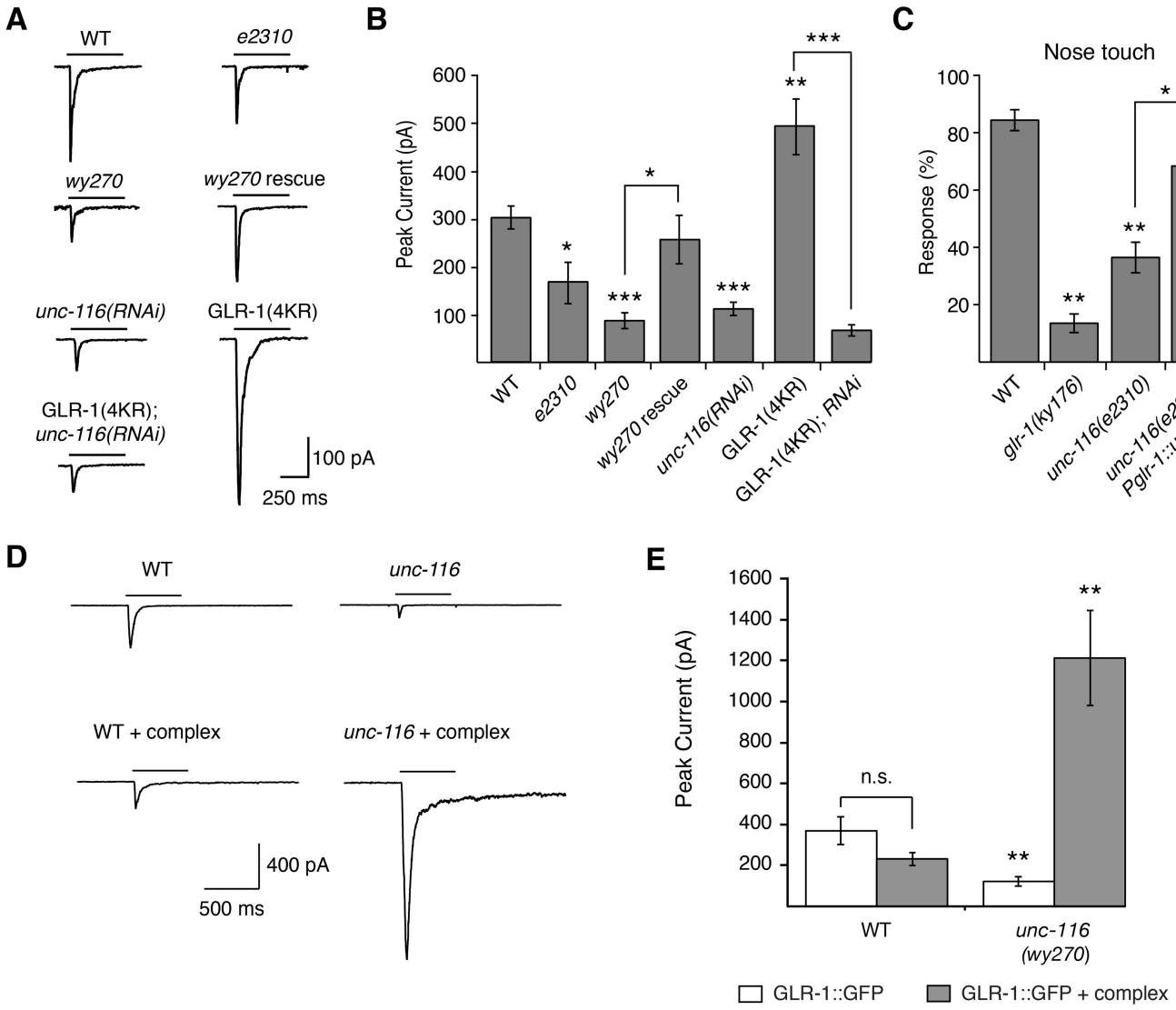

Figure 7. Glutamate-gated currents are reduced in *unc-116* mutants

(A) Representative traces of glutamate-gated currents in AVA of transgenic worms that expressed GLR-1: :GFP or GLR-1(4KR): :GFP. (B) Quantification of glutamate-gated currents. For all genotypes, n≥6 worms. (C) Response to nose touch stimulation, n=10 worms. (D) Glutamate-gated currents in AVA of transgenic worms that overexpressed GLR-1: :GFP either with or without overexpression of the GLR-1 signaling complex (complex = SOL-1 + SOL-2 + STG-2 + GLR-2). (E) Quantification of glutamate-gated currents. For all genotypes, n≥5 worms. ** p<0.01 significantly different from WT. * p<0.05; ** p<0.01; *** p<0.001. For all recordings, cells were held at −60 mV. Bars indicate 3 mM glutamate application. Error bars indicate SEM.

See also Figure S9.

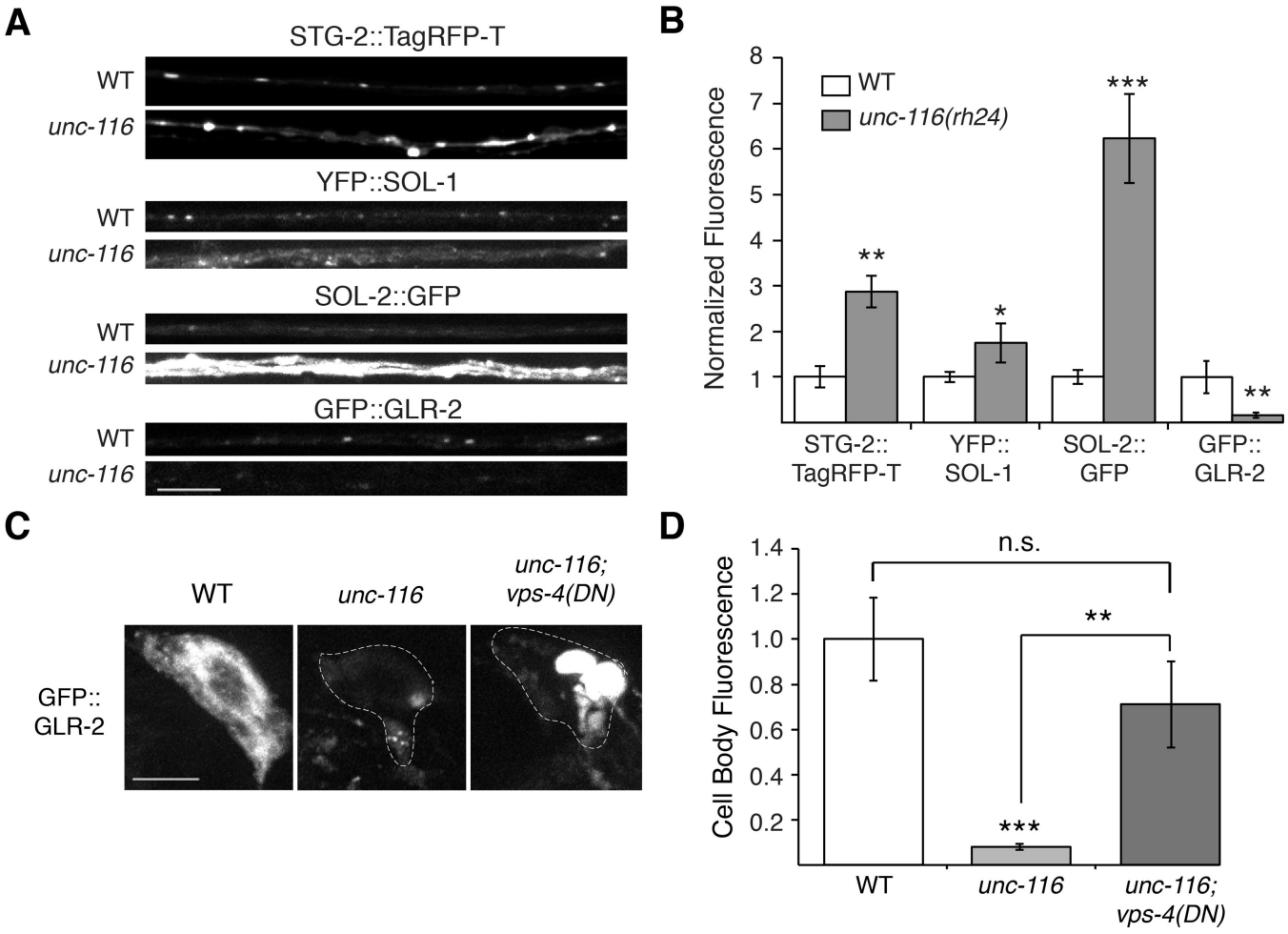

Figure 8. GLR-2 is decreased in *unc-116* mutants

(A) Confocal images of STG-2: :TagRFP-T, YFP: :SOL-1, SOL-2: :GFP and GFP: :GLR-2 in the AVA processes in transgenic WT and *unc-116(rh24)* mutants. (B) Quantification of synaptic puncta fluorescence normalized to WT, n>15 worms. (C and D) Confocal images of GFP: :GLR-2 in the AVA cell bodies (C) and corresponding quantification (D) in WT, *unc-116(rh24)* and *unc-116(rh24); vps-4(DN)* double mutants. For all genotypes, n≥8 worms.

* p<0.05, ** p<0.01, *** p<0.001. Scale bars represent 5 μm. Error bars indicate SEM.

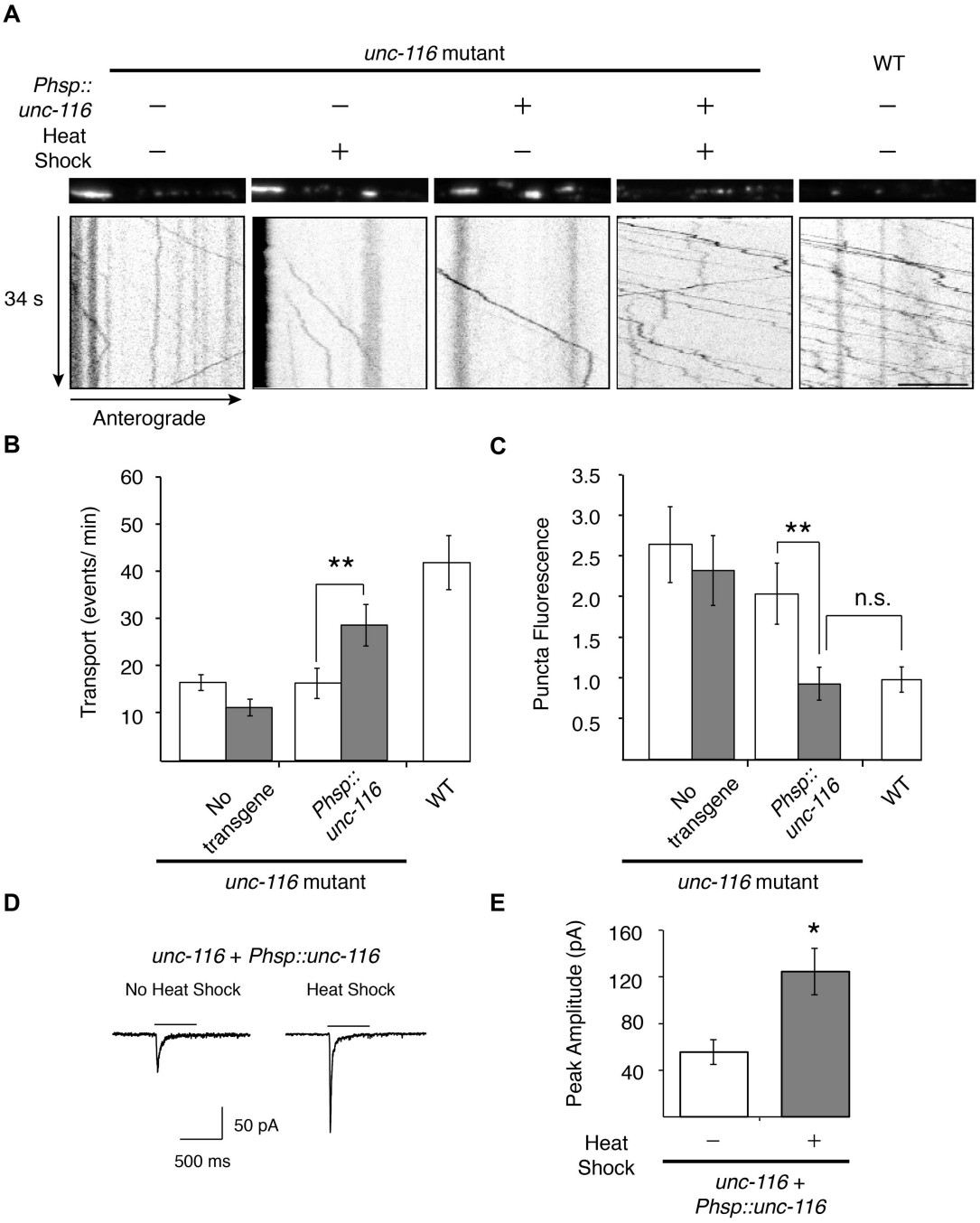

Figure 9. Transient expression of UNC-116/KIF5 in adult *unc-116* mutants rescues GLR-1 transport and synaptic transmission

(A) GLR-1: :GFP confocal images (top) and kymographs (bottom) in WT and *unc-116(wy270)* mutants in various treatment conditions. (B and C) Quantification of GLR-1: :GFP transport events per minute (B) and synaptic puncta fluorescence intensity (C) in worms with (grey) or without (white) heat-shock treatment normalized to WT, n=15 worms. Scale bar represents 5 μm. (D) Representative traces of glutamate-gated currents in AVA in transgenic *unc-116(wy270); Phsp: :unc-116* worms either with (right) or without (left) heat-shock treatment. Bars indicate 3 mM glutamate application. Cells were held at

−60 mV. (E) Quantification of glutamate-gated currents in worms with (grey) or without (white) heat-shock treatment. For all genotypes, n≥5 worms.
* p<0.05, ** p<0.01. Error bars indicate SEM.